Environmental Health Perspectives
Vol. 86, pp. 37–48, 1990

Morphology of Neoplastic Lesions Induced by 1,3-Butadiene in B6C3F$_1$ Mice

by Rodney A. Miller* and Gary A. Boorman†

1,3-Butadiene (CAS No. 106-99-0) was studied for potential carcinogenicity and chronic toxicity by inhalation in B6C3F$_1$ mice. Groups of 50 mice of each sex were exposed to 0, 625, or 1250 ppm 1,3-butadiene for 6 hr/day, 5 days/week for 60 weeks (male) or 61 weeks (female). The study was scheduled for 104 weeks of exposure but was terminated early because of reduced survival related to induction of a variety of tumors in 1,3-butadiene-exposed mice. A second chronic inhalation study was conducted in which male and female mice were exposed to 0, 6.25, 20, 62.5, 200, or 625 ppm for up to 2 years. Additional groups of 50 male mice were exposed to 625 ppm for 13 or 26 weeks, 312 ppm for 52 weeks, or 200 ppm for 40 weeks, then held without exposure until scheduled sacrifice 104 weeks after initial exposure.

1,3-Butadiene-exposed mice from both studies had increased incidences of malignant lymphomas that were observed as early as week 20 in the first study and week 23 in the second study. The lymphomas were primarily lymphocytic and originated in the thymus, although generalized lymphoma was often present. Exposed mice in both studies developed cardiac hemangiosarcomas that were observed as early as week 32 in the first study and week 41 in the second study. Also present were foci of endothelial hyperplasia in the myocardium that were regarded as early evidence of developing hemangiosarcoma. Alveolar epithelial hyperplasia, alveolar/bronchiolar adenomas and alveolar/bronchiolar carcinomas represented the spectrum of proliferative lung lesions induced by exposure to 1,3-butadiene in both studies. Exposure-related proliferative forestomach lesions observed in both studies included epithelial hyperplasia, squamous cell papillomas, and squamous cell carcinomas. 1,3-Butadiene-exposed female mice in both studies developed mammary gland neoplasms at increased incidences. Most of the mammary tumors were pleomorphic adenocarcinomas, but several adenoacanthomas were also seen. Granulosa cell tumors of the ovary were exposure-related neoplasms in both studies. Occasionally the granulosa cell tumors were malignant as evidenced by vascular invasion or pulmonary metastasis. Although there was an increased incidence of hepatocellular neoplasms in exposed females in the first study, by week 65 of the second study there was not evidence of a clear response of liver neoplasms. The preliminary results of the second study indicate there was induction of tumors similar to those seen in the first study but occurring in response to lower concentrations of 1,3-butadiene.

Introduction

1,3-Butadiene is a colorless, low molecular weight, reactive gas used in the production of styrene-butadiene or synthetic rubber (*1*). 1,3-Butadiene is mutagenic to *Salmonella typhimurium* strains (TA1530 and TA1535), and mutagenicity of butadiene requires metabolic activation (*2*). 1,3-Butadiene exerts strong genotoxic and cytotoxic effects on mouse bone marrow cells, resulting in an increase in frequency of circulating micronuclei, chromosomal aberrations, sister chromatid exchanges and circulating polychromatic erythrocytes; and a depressed cellular proliferation and depression of the mitotic index (*3–5*).

In a 2-year inhalation toxicity/carcinogenicity study of 1,3-butadiene at 1000 and 8000 ppm in Sprague-Dawley rats, 1,3-butadiene was considered a weak carcinogen. High concentration-exposed male rats had increased incidences of Leydig-cell tumors of the testis and pancreatic exocrine adenomas. At both exposure concentrations, female rats had increased incidences of mammary tumors and uterine sarcomas; they also had increased incidences of thyroid follicular cell adenomas and Zymbal gland tumors, when exposed to 8000 ppm 1,3-butadiene (*6*).

A chronic inhalation study designed for 104 weeks of exposure, in which B6C3F$_1$ mice were exposed to 625 or 1250 ppm of 1,3-butadiene, was terminated early (after 60–61 weeks of exposure) because of tumor-related mortality in all 1,3-butadiene exposed mice (*7,8*). There were early induction and significantly increased incidences of malignant lymphomas, cardiac hemangiosarcomas, alveolar/bronchiolar neoplasms, and squamous cell neoplasms of the forestomach in males and females and adenocarcinomas of the mammary gland, granulosa cell tumors of the ovary, and hepatocellular tumors in female

*Battelle, Pacific Northwest Laboratories, P.O. Box 999, LSL-II, Richland, WA 99352.
†*National Toxicology Program, National Institute of Environmental Health Sciences*, Research Triangle Park, NC 27709.
Address reprint requests to R. Miller, Battelle Pacific Northwest Laboratories, P.O. Box 999, LSL-II, Richland, WA 99352.

mice (*7,8*). Brain tumors and preputial gland carcinomas in male mice and Zymbal gland carcinomas in both sexes of mice were seen at low incidences but, because of their rare occurrence in untreated mice, they were suggested to have been possibly related to treatment (*7–9*).

A second chronic study was conducted in which preliminary results indicate there is induction of similar tumors at the same sites seen in the first study, and tumor induction in the second study is occurring at lower concentrations than seen in the first 1,3-butadiene study. This paper documents and describes the gross and microscopic characteristics of the pertinent, induced neoplastic processes observed after 60 to 65 weeks of exposure.

Materials and Methods

The neoplastic processes described in this paper were those observed during the first 1,3-butadiene study that was conducted according to published literature (*7,8*) and those observed during the second 1,3-butadiene study conducted under similar conditions but at different exposure concentrations. Male and female mice in the second study were exposed to 0, 6.25, 20, 62.5, 200, or 625 ppm of 1,3-butadiene for up to 2 years. Interim sacrifices were done at 40 and 65 weeks on these mice. Additional groups of 50 male mice were exposed to 625 ppm for 13 or 26 weeks, 312 ppm for 52 weeks, or 200 ppm for 40 weeks, then held without exposure until scheduled sacrifice 104 weeks after initial exposure. Preliminary findings on the second study come primarily from early death animals before the 65-week interim sacrifice. Histopathologic diagnoses were made by light microscopic examination of tissues fixed in 10% neutral buffered formalin, embedded in paraffin, sectioned at 5 to 6 μm, and stained with hematoxylin and eosin.

Results and Discussions

Malignant Lymphoma

Exposure of mice to 1,3-butadiene resulted in increased incidences of malignant lymphomas in both sexes, and they were observed as early as week 20 in the first 1,3-butadiene study and week 23 in the second study. Most malignant lymphomas seemed to originate in the thymus, which is different from spontaneous lymphomas observed in this strain of mouse (*10*). The thymus was the most frequently and prominently affected organ and occasionally the only affected organ. The typical gross appearance of malignant lymphoma was a large, pale, firm anterior mediastinal mass, displacing other thoracic cavity organs and often accompanied by hydrothorax (Fig. 1). While thymic involvement of malignant lymphoma was predominant, generalized lymphoma was often encountered in the spleen, various lymph nodes, liver, kidney, lung, and less frequently in other organs. Most of the malignant lymphomas were well differentiated and lymphocytic (Fig. 2), a few were undifferentiated (*11*). The lymphocytic malignant lymphomas formed monotonous sheets of uniform small to medium-size lymphocytes with round nuclei and little cytoplasm that focally or diffusely infiltrated the various organs. Malignant lymphoma was considered the major cause of early deaths in these studies.

1,3-Butadiene-induced thymic lymphoma cells have been shown to possess surface markers indicative of early T-lymphocytes and to have elevated amounts of murine leukemia virus (*12*). The role of endogenous ecotropic retrovirus and 1,3-butadiene in this system has not yet been fully elucidated (*13*).

A few malignant lymphomas were diagnosed as histiocytic. They differed from the lymphocytic type in that

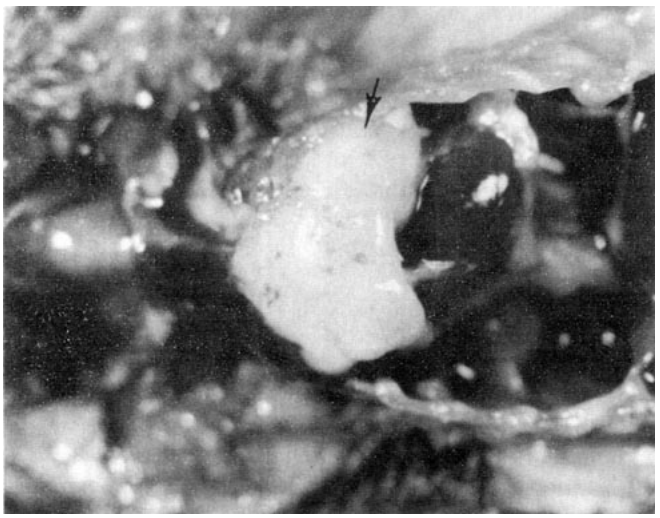

FIGURE 1. Thymic lymphoma as typically observed at necropsy. The white mass (arrow) is neoplastic thymic tissue occupying the anterior thoracic cavity.

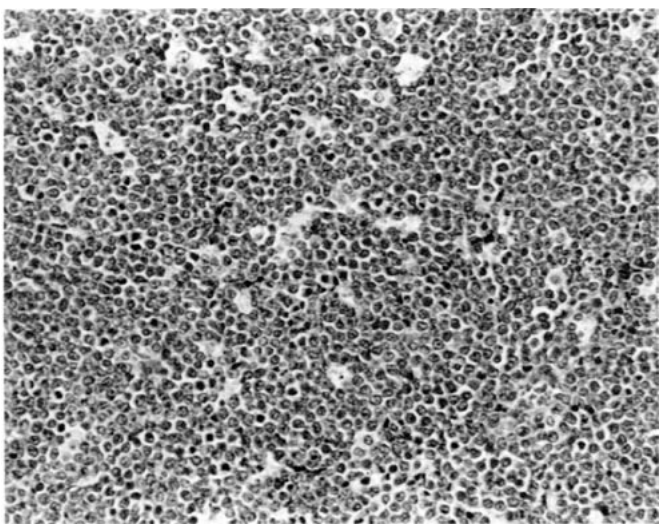

FIGURE 2. Photomicrograph of thymic lymphoma composed of a uniform monotonous sheet of small to medium-sized lymphocytes. Original magnification, ×50.

they tended not to involve the thymus but typically affected the liver, spleen, lymph nodes, lung, and kidneys. Histologically, they were characterized by larger, variably sized cells with abundant eosinophilic cytoplasm and oval- to bean-shaped nuclei and occasional giant cells. A third distinct type of lymphoma encountered was mixed-cell lymphoma, it was typically seen as an enlarged mesenteric lymph node. Mixed-cell lymphomas were even less common than histiocytic lymphomas and were characterized by the presence of scattered large, pale, reticular cells intermixed with small lymphocytes and plasma cells.

Cardiac Hemangiosarcomas

Hemangiosarcomas of the heart were seen in both sexes and were first observed as early as week 32 in the first study and around week 41 in the second study. Gross lesions of hemangiosarcoma were generally very distinctive. Affected mice sometimes had red fluid in the thoracic cavity. Heart masses, when observed grossly, were generally described as pale or red and 1 mm to 9 mm in diameter. The masses occurred within ventricular muscle at any location but more frequently at the apex of the heart. Occasionally, the heart masses protruded from the epicardial surface as dark saclike lesions (Fig. 3), sometimes adherent to the lung. Commonly, heart hemangiosarcomas were deep within the myocardium and not visible grossly even at trimming. Metastatic pulmonary hemangiosarcomas were observed as distinctive multifocal 1 mm diameter red or dark foci at necropsy (Fig. 4). Metastatic liver lesions were seen more frequently than metastatic lung lesions and occasionally were the only gross evidence of hemangiosarcoma. The liver lesions had the characteristic gross appearance of multiple red or dark, soft, or friable foci 1 to 3 mm in diameter. The liver lesions were cystic and filled with dark red fluid (Fig. 5). Occasionally a larger cystic lesion would rupture and cause hemoperitoneum.

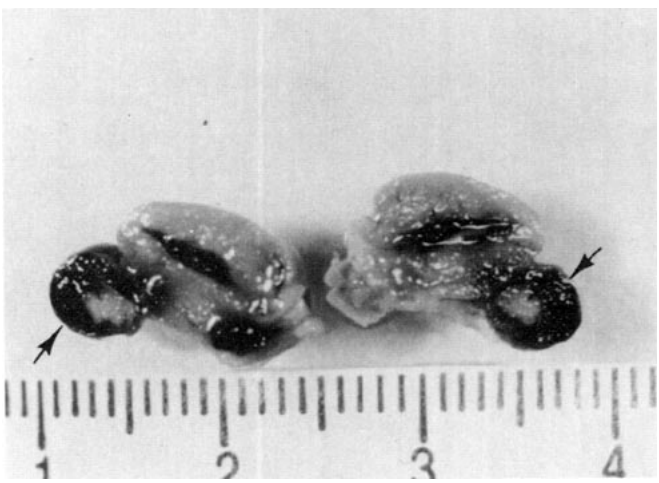

FIGURE 3. Cardiac hemangiosarcomas occasionally were observed at necropsy to erode through the epicardium to form dark masses of tumor tissue, hemorrhage, and thrombus (arrows).

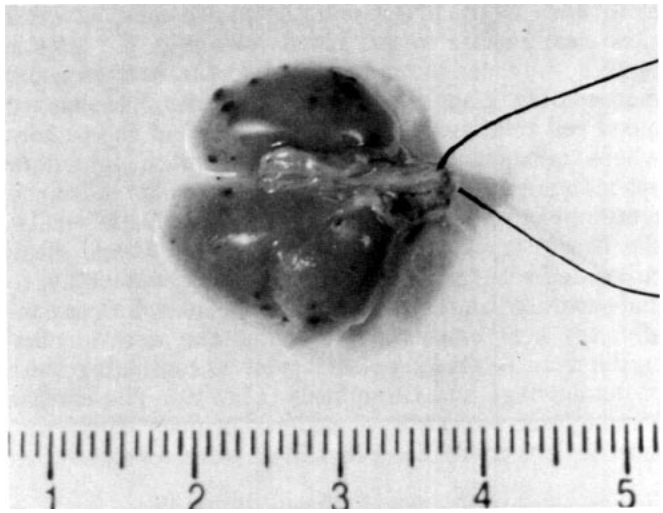

FIGURE 4. Metastatic pulmonary hemangiosarcoma as seen at necropsy. Multiple small, dark foci were scattered through the lung.

FIGURE 5. Dark, pitted, punctate foci were characteristic of liver hemangiosarcoma seen at necropsy.

Microscopically, hemangiosarcomas of the heart occurred in all ventricular locations. The heart tumors varied considerably in size and histologic character. The earliest detectable lesion associated with development of cardiac hemangiosarcoma was diagnosed as endothelial hyperplasia. This hyperplastic lesion was characterized by small intramyocardial foci of prominent plump or swollen endothelial cells lying in a single layer on the endomysium between seemingly shrunken myofibers (Fig. 6). Space between adjacent myofibers was increased, resulting in a clear space that sometimes contained red blood cells. When endothelial cells became more pleomorphic and began to pile up; then the diagnosis of hemangiosarcoma was made. Advanced lesions typically had solid foci of anaplastic, pleomorphic, rounded to elongated cells with large vesicular nuclei and prominent nucleoli. The foci had various sized tissue

clefts lined by the plump endothelial like cells, having a close relationship to red blood cells (Fig. 7). Mitotic figures were common. Frequently, the masses could more readily be appreciated as having an endothelial/red blood cell relationship at the periphery of the tumors where tissues had a looser structure, and the interfiber spaces were wider, and the plump endothelial cells lined more obvious vascular channels (Fig. 8). Occasionally, the heart tumors were multifocal (Fig. 9) and often co-existed with foci of endothelial hyperplasia distant to and separate from the main cardiac neoplasm. Occasionally, the hemangiosarcoma invaded the visceral pericardium and formed neoplastic growths containing areas of hemorrhage and thrombosis (Fig. 10). The cardiac hemangiosarcomas were considered primary. However, most lesions in the lung and liver were considered as metastatic because early lesions were observed in the heart and rarely at other sites, the incidence was highest in the heart, and pulmonary or liver hemangiosarcoma were rarely observed in the absence of cardiac tumors. Hemangiomatous liver lesions were characterized by multifocal cystic structures filled with red blood cells (Fig. 11). The liver lesions typically had single to multi-

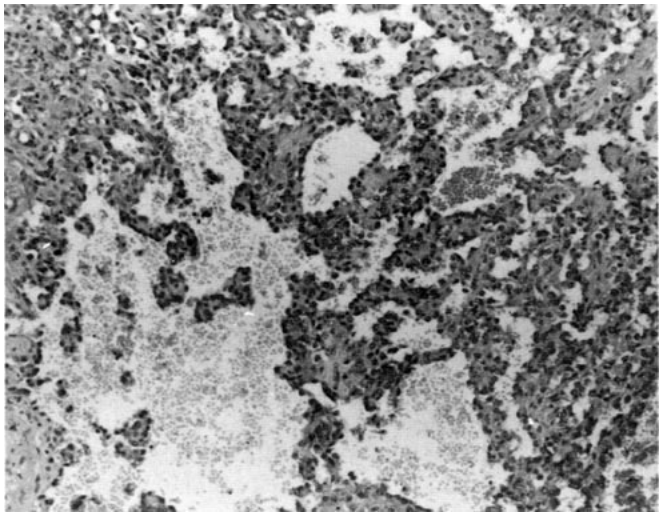

FIGURE 6. Endothelial hyperplasia characterized by increased prominence of plump, dark cells (arrow) lining muscle fibers along enlarged clear spaces. Original magnification, ×50.

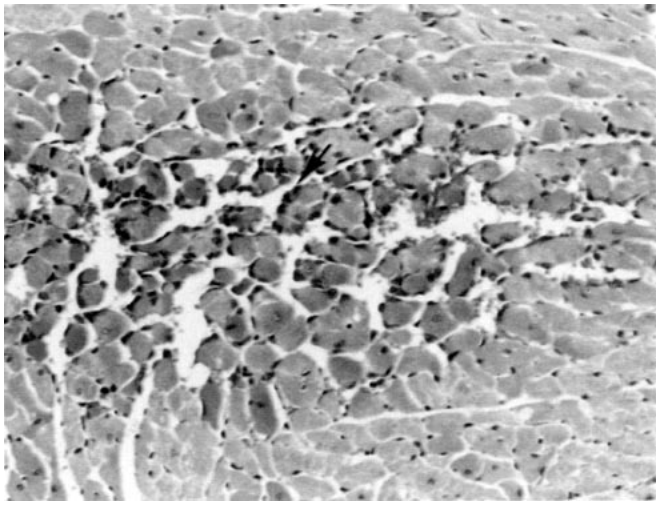

FIGURE 7. Anaplastic cardiac hemangiosarcoma having solid foci of neoplastic cells and variably-sized vascular clefts, some of which contain red blood cells. Original magnification, ×50.

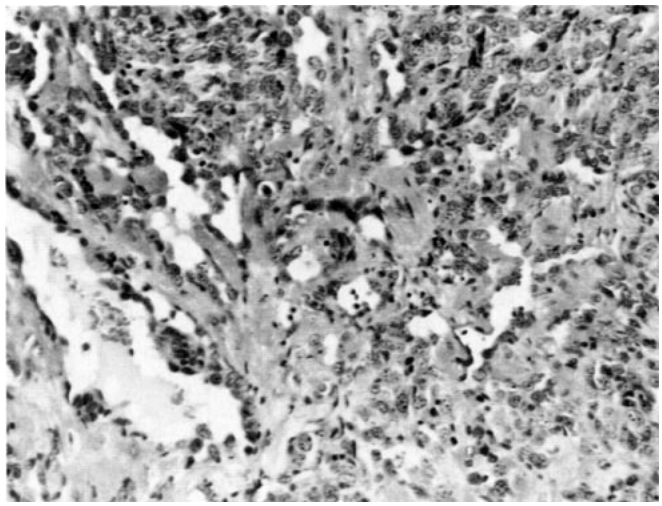

FIGURE 8. Cardiac hemangiosarcoma with larger, more obvious, vascular spaces lined by endothelial cells and filled with red blood cells. Original magnification, ×33.

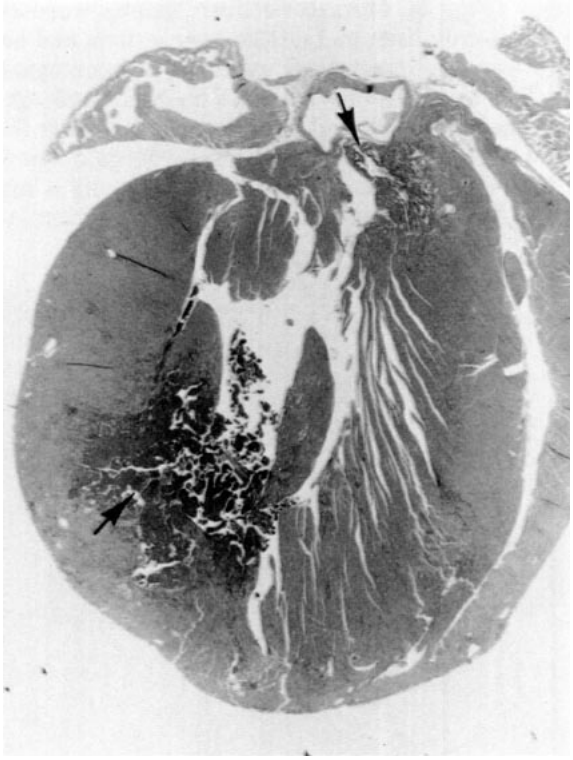

FIGURE 9. Cardiac hemangiosarcomas within myocardium and not visible at necropsy. This heart had two hemangiosarcomas at some distance from each other (arrows). Original magnification, ×2.5.

FIGURE 10. Cardiac hemangiosarcoma with hemorrhage and thrombosis at the apex of the heart (arrow). Original magnification, ×2.5.

layered tumor cells lining the cystic areas and lining cords of hepatocytes that projected into and across the cyst lumina. Infrequently, solid foci of tumor cells were observed in the liver. Metastatic lung lesions were characterized by multifocal areas of hemorrhage around vascular channels lined by spindle cells and some solid sarcoma cell emboli (Fig. 12). Infrequently, metastatic hemangiosarcoma cells were found in glomerular tufts and the brain.

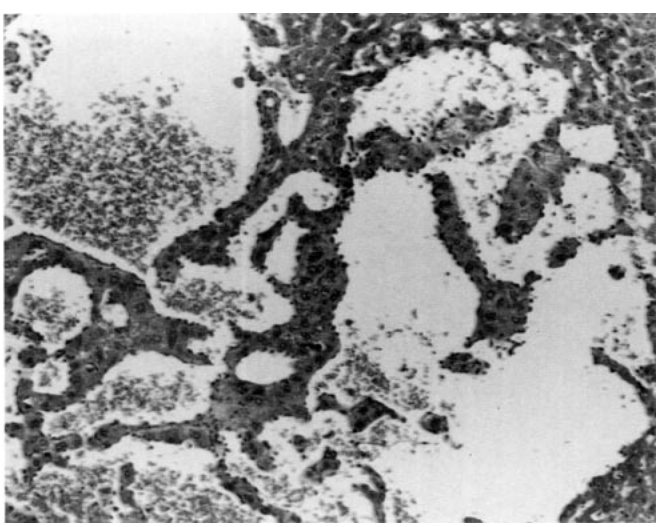

FIGURE 11. Hepatic hemangiosarcoma characterized by cystic spaces filled with red blood cells and lined by prominent endothelial cells. Original magnification, ×25.

Hemangiosarcomas of the heart are rare in the mouse (*9,10,14*) with a 0.04% incidence in $B6C3F_1$ mice (*7*). Ultrastructural characteristics of 1,3-butadiene-induced cardiac hemangiosarcomas have been described (*15*).

Proliferative Lung Lesions

Grossly, proliferative lung lesions in both sexes of each study were usually observed as white or pale nodules 1 to 3 mm in diameter. The smaller foci and nodules tended to correlate with alveolar bronchiolar epithelial hyperplasia or adenomas. Larger, pale, firm lung masses tended to correlate with alveolar/bronchiolar carcinomas that occupied whole lung lobes and were as large as 1.5 cm in diameter (Fig. 13).

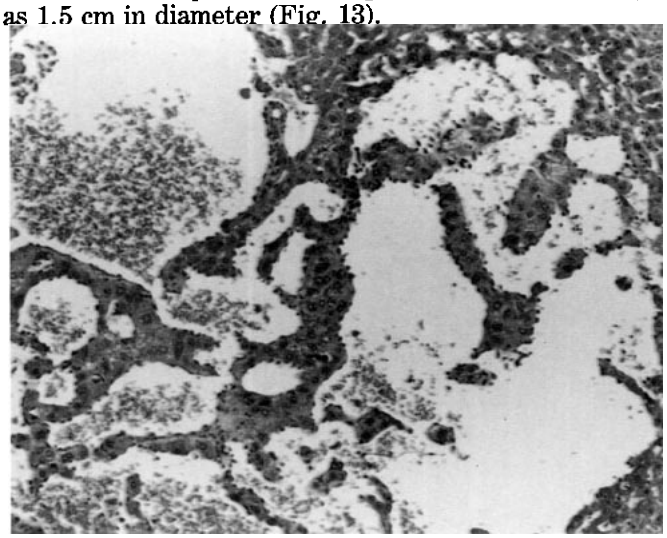

FIGURE 12. Lung with metastatic hemangiosarcoma having a focus of hemorrhage and spindle cell proliferation (double arrows) and an embolus of neoplastic cells (single arrow). Original magnification, ×33.

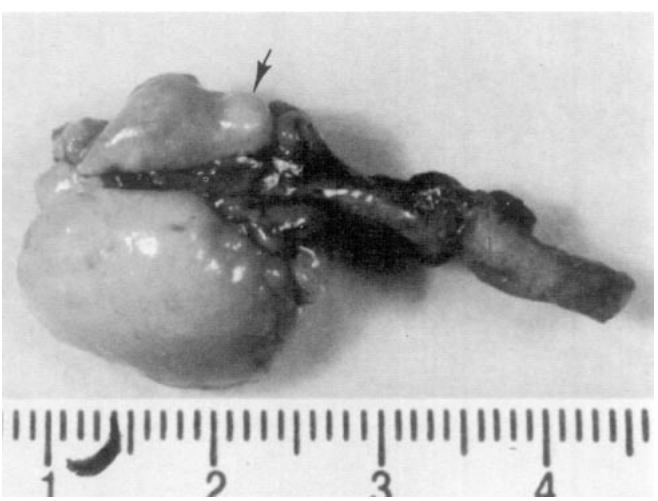

FIGURE 13. Alveolar/bronchiolar carcinomas as seen at necropsy. A large diaphragmatic lobe mass occupies the whole right side (nearest the ruler) and a smaller mass is present in the left lobe (arrow).

Alveolar epithelial hyperplasia was usually characterized by focal proliferation of cuboidal epithelial cells in alveolar areas (Fig. 14) with basic alveolar architecture remaining intact; occasionally, a more columnar-shaped cell proliferated along alveolar ducts (Fig. 15). Alveolar/bronchiolar adenomas were diagnosed when compression of adjacent tissue and loss of alveolar structure were observed (Fig. 16). When lung tumors displayed increased pleomorphism and showed evidence of tissue invasion or metastasis, alveolar/bronchiolar carcinomas were diagnosed. Alveolar/bronchiolar carcinomas were frequently papillary and commonly had areas of cuboidal proliferation (Fig. 17) interposed with areas of a more columnar cell with elongated palisading nuclei. Alveolar/bronchiolar carcinomas were rarely metastatic. The alveolar/bronchiolar tumors were typical of those encountered in the mouse (*16*) and also called alveologenic or bronchiolar/alveolar tumors. They are generally accepted as arising primarily from alveolar Type II cells and/or Clara cells; other types of tumors were considered rare (*16,17*). A lung tumor, observed infrequently in the second 1,3-butadiene study and not observed in the first study, was an adenocarcinoma that tended to have areas of solid growth patterns; some of the columnar cells that formed acini were discrete goblet cells (Fig. 18). Portions of these tumors were highly anaplastic and tended to be invasive to the mediastinal cavity with frequent metastasis to the heart, kidney, and skeletal muscle.

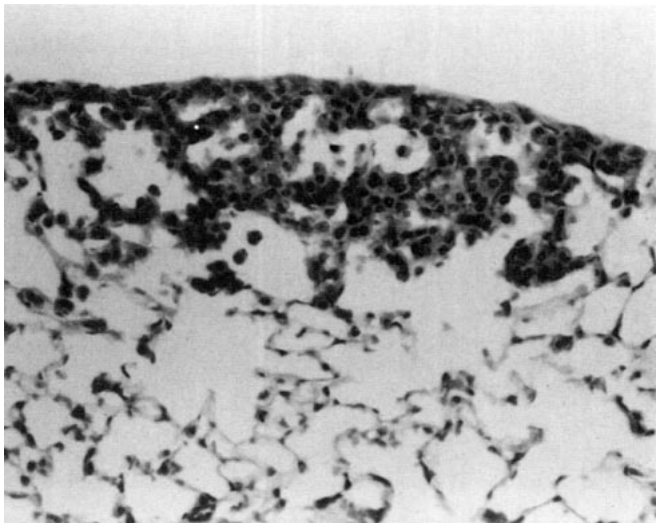

FIGURE 14. Alveolar epithelial hyperplasia with cuboidal lining cells and retention of basic architecture. Original magnification, ×66.

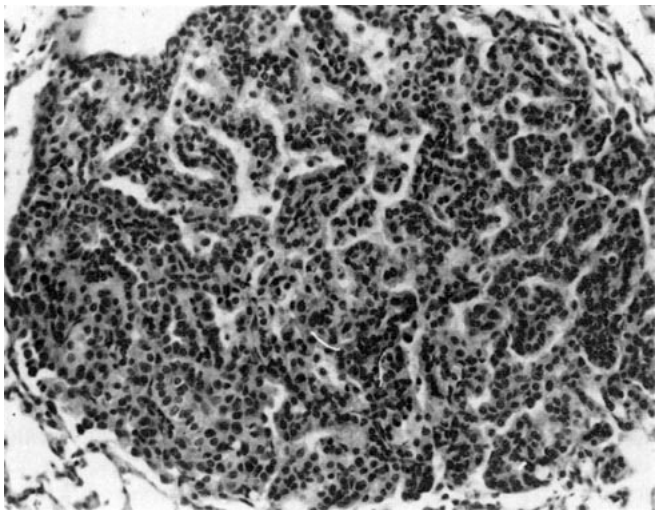

FIGURE 16. Alveolar/bronchiolar adenoma with a uniform cell population, peripheral tissue compression, and loss of basic alveolar architecture. Original magnification, ×50.

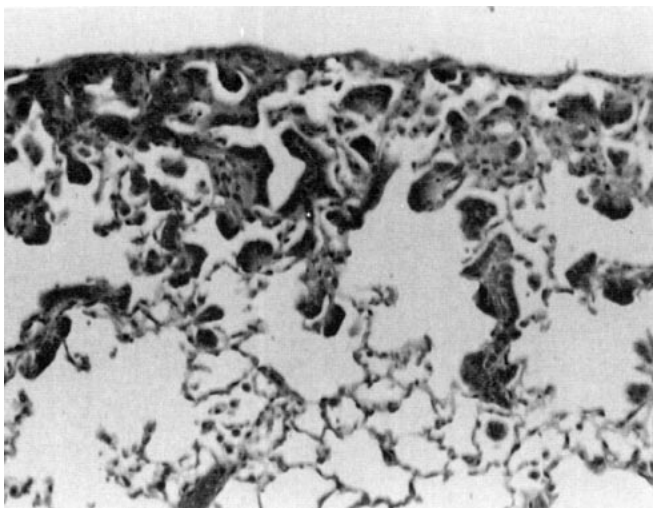

FIGURE 15. Alveolar epithelial hyperplasia with a more columnar lining cell. Original magnification, ×50.

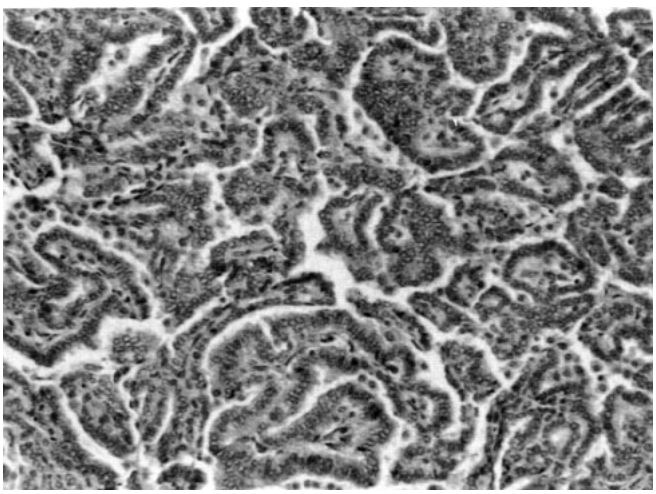

FIGURE 17. Alveolar/bronchiolar carcinoma having prominent cellular pleomorphism and increased nucleus to cytoplasmic ratio. Original magnification, ×50.

Forestomach Squamous Cell Proliferative Lesions

Both sexes of mice in each study had increased incidences of proliferative forestomach lesions. Forestomach epithelial hyperplasia at necropsy was a thick, white, pale, focus or raised lesion 1 to 2 mm in diameter. Squamous cell papillomas were similarly described but tended to be larger. Squamous cell carcinomas of the forestomach were often described as pale, firm 1.5- to 2.0-cm masses penetrating the forestomach wall and growing as multiple nodules on the serosal surface and occasionally seeding throughout the peritoneal cavity (Fig. 19).

Forestomach epithelial hyperplasia was an occasionally diffuse but usually a focal lesion of folded hyperkeratotic epithelium with rete peg formation (Fig. 20). Occasionally, ulcers or microabscesses were present in the hyperplastic foci. Squamous cell papillomas were also common. They were variable in complexity from two to three fingerlike projections of epithelial growths to multipronged, villous masses having many exophytic projections of fibrovascular cores covered with acanthotic, hyperkeratotic squamous epithelium (Fig. 21). Squamous cell carcinomas were diagnosed when there was invasion of the muscularis by proliferating squamous epithelium. These neoplasms were generally well differentiated (Fig. 22), but occasionally more anaplastic, with the only evidence of squamous differentiation seen as tiny keratin pearls scattered among

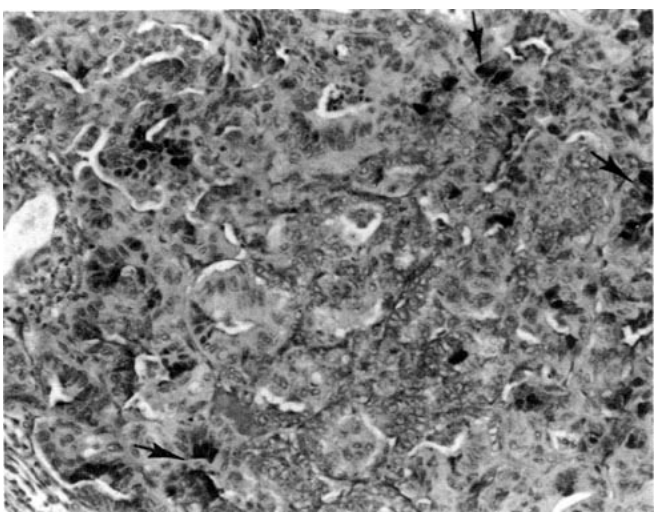

FIGURE 18. Pulmonary adenocarcinoma demonstrating pleomorphic epithelial cells, some of which are goblet cells (arrows). PAS stain. Original magnification, ×50.

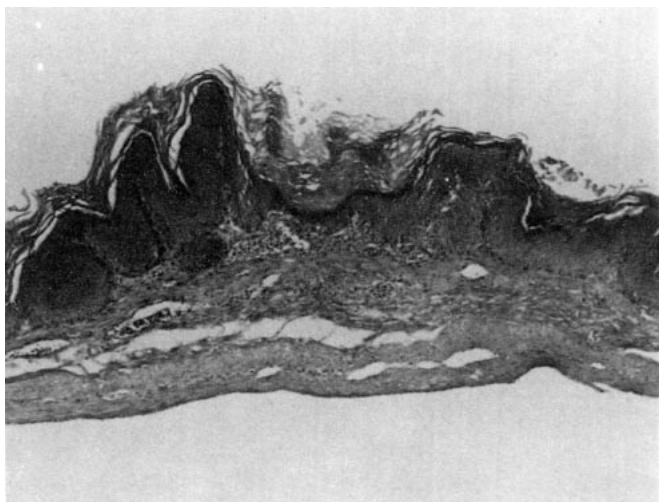

FIGURE 20. Epithelial hyperplasia of the forestomach having a focally folded and thickened epithelium with concurrent hyperkeratosis. Original magnification, ×16.

FIGURE 19. Squamous cell carcinoma of the forestomach invading through the forestomach wall (arrows) and growing on serosal surfaces.

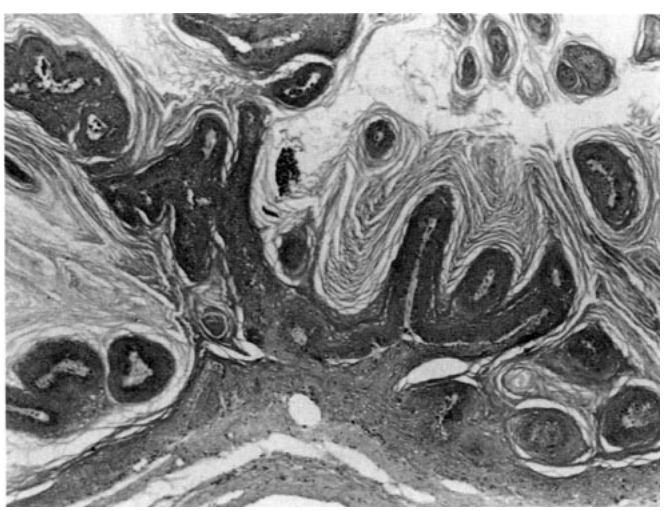

FIGURE 21. Forestomach squamous cell papilloma having multiple exophytic projections of fibrovascular cores covered with hyperkeratotic squamous epithelium. Original magnification, ×16.

the neoplastic cells. A few of the squamous cell carcinomas had a focal sarcomatous appearance. Squamous cell papillomas of the forestomach occur in only 0.3% of control male $B6C3F_1$ mice and 0.5% of control female $B6C3F_1$ mice and squamous cell carcinomas are even less common (*9,10*).

Mammary Gland

Mammary gland neoplasms in females from both studies were generally described as subcutaneous skin masses that were pale, firm, rubbery, and 2 to 3 cm in diameter. Because of different pathology data collection systems, acinar cell carcinoma of the first study was diagnosed as adenocarcinoma in the second study, while adenosquamous carcinoma in the first study was diagnosed as adenoacanthoma in the second study. The mammary adenocarcinomas usually had fields of small acini lined by large pleomorphic, cuboidal to polygonal epithelial cells (Fig. 23). However, morphologic characteristics of the adenocarcinomas were highly variable within the same tumor and between tumors. Patterns encountered included: papillary, cystic, solid cords, sheets, bands, and comedo. Mammary adenocarcinomas usually had multiple growth patterns, but occasionally a single pattern prevailed throughout the tumor section. Metastases to the lung were not unusual.

Adenoacanthoma was another type of mammary tumor that could be separated morphologically from the adenocarcinomas because of its distinctive squamous component. Adenoacanthomas, by definition, are malignant mammary tumors with over 25% of its composition being squamous cell differentiation (*18,19*). Adenoacanthomas had a glandular component similar to mammary adenocarcinomas, but tumor cells lining some of the acini underwent squamous differentiation and keratinization (Fig. 24). Pulmonary metastasis of the mammary adenoacanthomas was not uncommon.

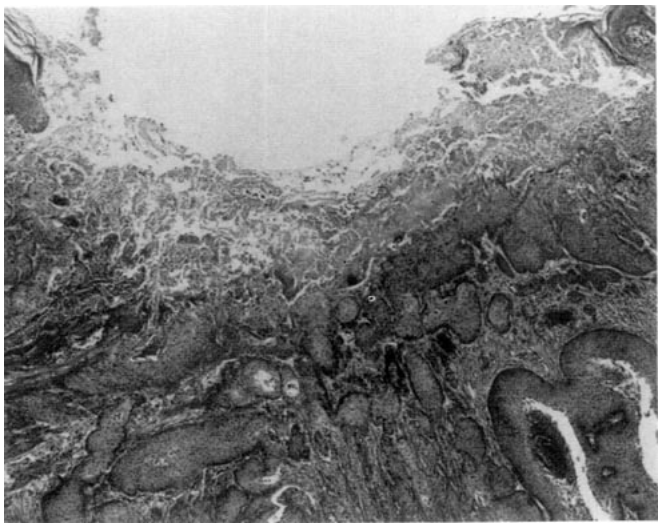

FIGURE 22. Squamous cell carcinoma of the forestomach growing into the muscle layers beneath an ulcerated epithelium. Original magnification, ×10.

Ovarian Granulosa Cell Tumors

Granulosa cell tumor induction was treatment-related in both 1,3-butadiene studies. Grossly, granulosa cell tumors were described as masses or enlarged ovaries that were yellow, pale, firm, and 3 to 6 mm in diameter. Occasionally, they were described as red, firm masses 1 to 1.5 cm in diameter.

Granulosa cell hyperplasia was observed in a small number of animals where the focal increase in granulosa cells was noncompressive and occupied less than half of the ovary. Granulosa cell tumors observed thus far varied considerably in size and morphology. Most of the granulosa cell tumors were benign. Small granulosa cell tumors were diagnosed when they compressed or com-

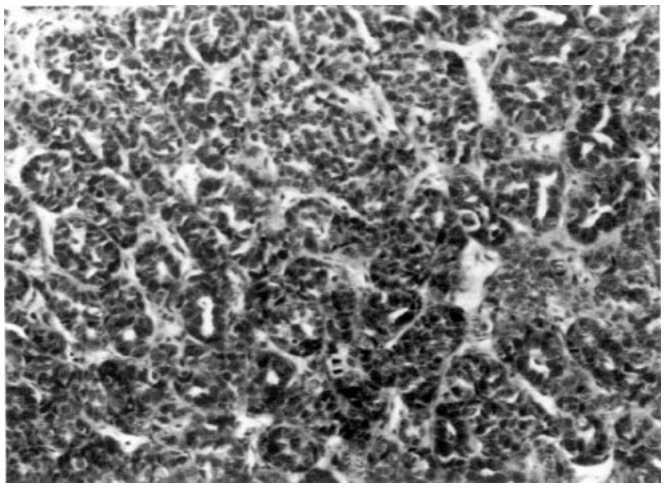

FIGURE 23. Mammary gland adenocarcinoma. Most mammary adenocarcinomas, although extremely pleomorphic, had some portions similar to this photomicrograph. Note the small acini lined by anaplastic epithelial cells. Original magnification, ×50.

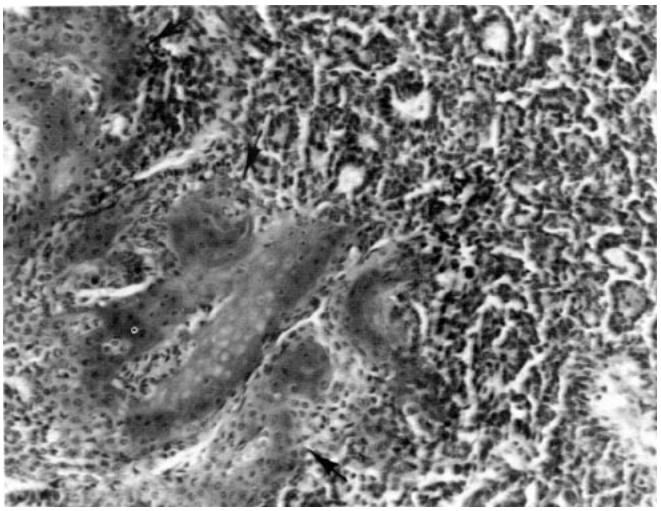

FIGURE 24. Mammary gland adenoacanthomas contained prominent areas of squamous differentiation (arrows) in addition to areas similar to the adenocarcinomas. Original magnification, ×50.

pletely displaced surrounding ovarian tissue (Fig. 25). Usually they were composed of uniform proliferation of granulosa cells aligned on a scant fibrous stoma in a discretely packeted tubular pattern (Fig. 26). Occasionally the ovarian tumors were larger, forming cysts separated by thick fibrous trabeculae on which proliferating granulosa cells were located. Nests and islands of proliferating granulosa cells were often isolated within the trabeculae (Fig. 27). Cystic areas in these larger neoplasms were often filled with red blood cells or less often filled with clear or lacy fluid (Fig. 28). Call-Exner bodies or microfollicular patterns were not commonly seen. Occasionally, large malignant granulosa cell tumors were observed. Generally, they had increased mitotic figures and cellular pleomorphism. Some of the tumors showed vascular invasion and occasionally metastasized to the lung. Although other ovarian tumors (benign mixed adenoma, adenoma) were also noted, their incidences were low. Generally, in control B6C3F$_1$ mice granulosa cell tumors are the third most commonly encountered ovarian tumors (*20*) and they are expected to be seen in less than 0.5% of control mice (*9*).

Liver Neoplasms

In the first 1,3-butadiene study, the incidences of hepatocellular neoplasms were statistically increased in female mice, but a clear response is not present in the second 1,3-butadiene study at week 65. Grossly, liver tumors varied from nodules 3 mm in diameter to masses 2 cm in diameter (Fig. 29). They varied in color from pale

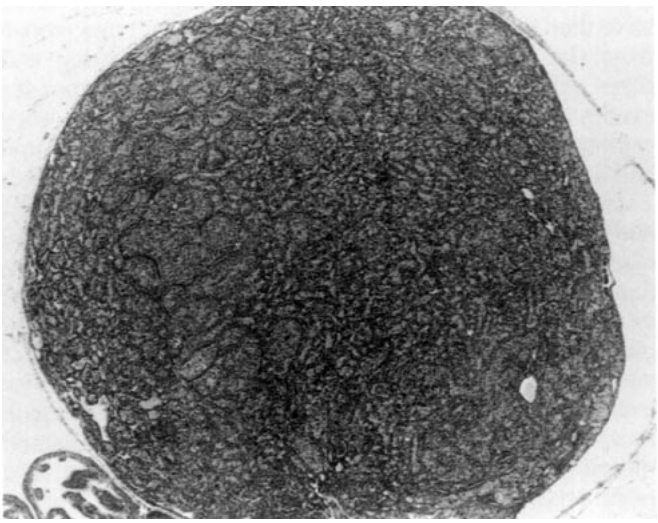

FIGURE 25. This photomicrograph represents one end of the spectrum of granulosa cell tumors, being small, solid, and uncomplicated. Original magnification, ×10.

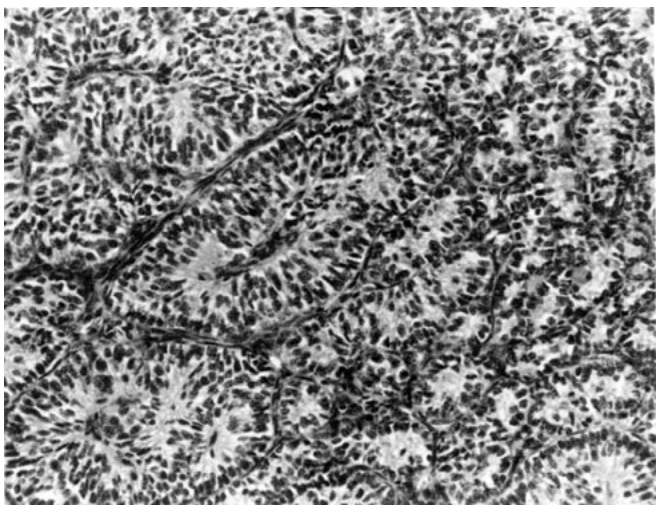

FIGURE 26. Higher magnification of Figure 25 shows uniform, regular, proliferation of granulosa cells along a scant fibrous stroma. Original magnification, ×50.

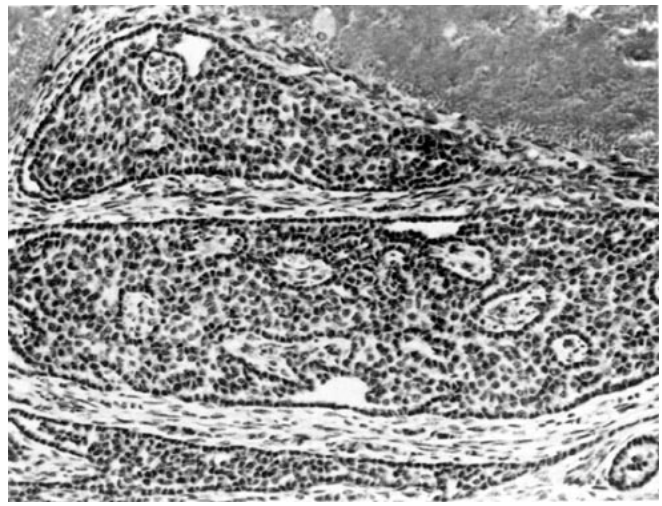

FIGURE 27. Photomicrograph of a large cystic granulosa cell tumor where the cystic areas are filled with red blood cells and proliferative granulosa cells are present within thick fibrous connective tissue bands. Original magnification, ×50.

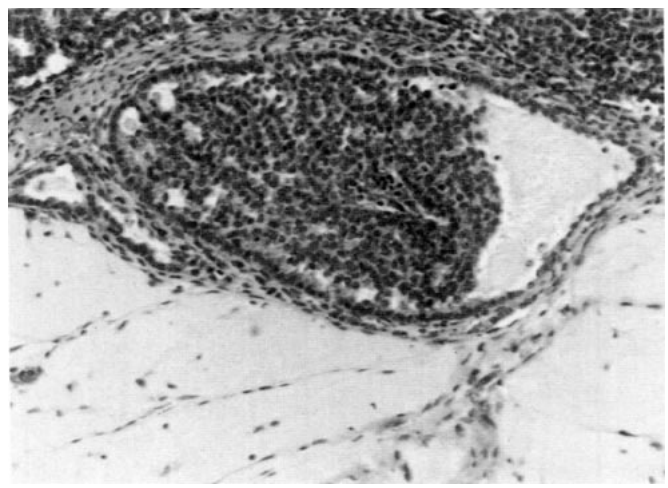

FIGURE 28. Granulosa cell tumor with thick fibrous bands separating islands of granulosa cells and cystic areas filled with amorphous debris. This tumor has a microfollicular pattern and has metastasized to the lung. Original magnification, ×50.

tan to mottled dark red and were seen in one or multiple lobes. Histologically, the morphologic variety observed in the hepatocellular adenomas and carcinomas was typical of that generally encountered in mice (*21*). Hepatocellular adenomas were generally smaller and composed of uniformly sized, well-differentiated cells having little nuclear pleomorphism (Fig. 30). Hepatocellular adenomas formed somewhat regular cords generally one cell thick and were sharply demarcated from the surrounding liver tissue by a compression zone. Hepatocellular carcinomas were typically, but not always, larger and characterized by a sharply demarcated proliferation of hepatocytes showing prominent nuclear pleomorphism and variability in cell size. Hepatocellular carcinomas usually had distinctly formed trabeculae many cells thick (Fig. 31). Hepatocellular carcinomas occasionally metastasized to the lung.

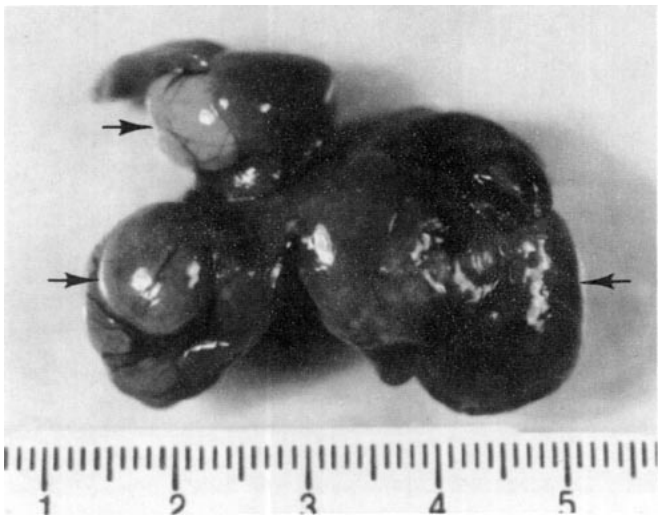

FIGURE 29. Necropsy photograph of a typical liver containing hepatocellular tumors (arrows).

Brain Tumors

Brain tumors were observed in the first 1,3-butadiene study in male mice (two exposed to 625 ppm and one exposed to 1250 ppm) (*7*). Since brain tumors are rare in mice (*9*), it was suggested that this may represent a treatment-related effect, especially since these lesions were seen in mice 66 weeks old or less. In the second 1,3-butadiene study, a few brain tumors were also found. Thus far, all were in males. Some similarities among the tumors have been observed. Grossly, the brain tumors usually affected the olfactory bulb and were observed as being 3 to 5 mm in diameter gray or pale, friable, or gelatinous masses. While only one mouse died before 65 weeks with a brain tumor, three have died since. To date the lesions represent one mouse from the 625 ppm 26 week stop-exposure group and three mice from the 625 ppm 13 week stop-exposure group, all of which had tumors involving the olfactory region. A male mouse exposed to 200 ppm for a lifetime had a brain tumor that was not in the olfactory region. Three of the four mice with olfactory bulb involvement had identical histologic patterns diagnosed as neuroblastomas. Histologically the tumors appeared as densely cellular, irregularly arranged sheets, columns, or packets of lymphocytelike cells within a sparse, lacy, poorly stained stroma (Fig. 32). There was a rare hint of pseudorosette formation. The fourth tumor had a similar cellular arrangement, but it had a loose spindle cell component as well. All four of the tumors also affected the olfactory region of the posterior nasal section, and some showed evidence of a meningeal compression as well as brain parenchyma invasion.

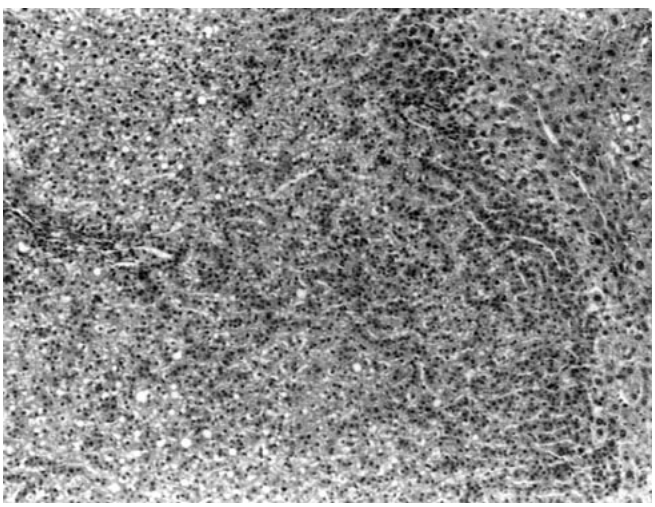

FIGURE 30. Hepatocellular adenoma (left portion of photograph) has a sharp line of demarcation with normal tissue. Neoplastic hepatocytes are uniform, and hepatic cords are regular and usually one-cell thick. Original magnification, ×25.

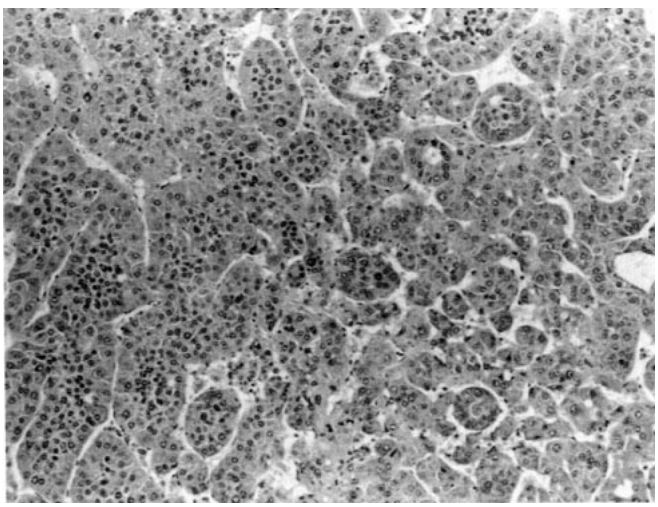

FIGURE 31. Hepatocellular carcinoma with marked cellular pleomorphism and distinct trabeculae. Original magnification, ×25.

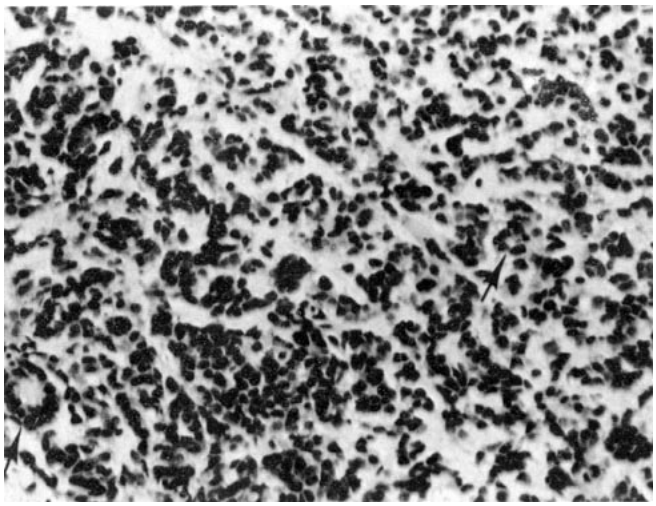

FIGURE 32. Neuroblastoma characterized by dense cellularity, irregular columns, rows, and packets of cells with little cytoplasm. Matrix is sparse, lacy, and poorly stained. Attempts at pseudorosette formation are noted (arrows). Original magnification, ×50.

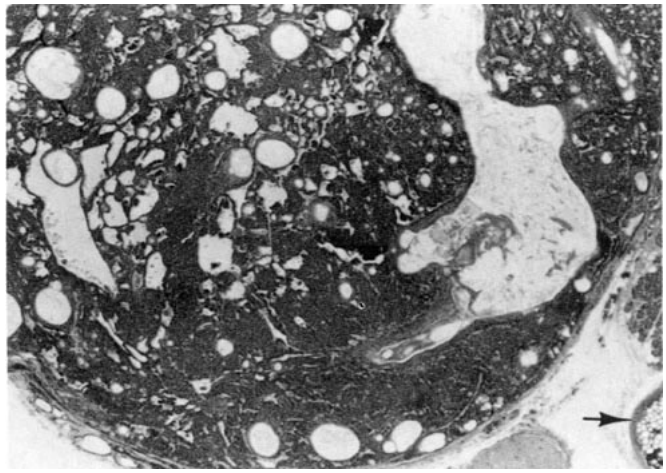

FIGURE 33. Zymbal gland adenoma seen as a compressive nodule next to ear canal cartilage (arrow). Original magnification, ×10.

Zymbal Gland Carcinomas

Zymbal gland carcinomas in the first 1,3-butadiene study, because of their rarity, were suggested to be possibily treatment-related (*7,9*). Zymbal gland carcinomas were seen in two males and one female exposed to 1250 ppm. Thus far, in the second study, one has been seen in a mouse exposed to 625 ppm for 26 weeks, and two have been observed in mice exposed to 625 ppm for 13 weeks. Two benign Zymbal gland tumors were seen in female mice exposed to 625 ppm.

Histologically, the Zymbal gland carcinomas were characterized by expansive multilocular areas of necrosis rimmed by viable, proliferating small basophilic cells that showed a tendency for squamous differentiation on the surface near the necrosis and around multiple small cystic foci scattered through the mass. Multiple foci of differentiation toward sebaceous cells were observed. Infiltration of surrounding tissues and blood vessels was observed, as well as metastasis to the lung. The benign tumors seen in the female mice were an adenoma and a duct papilloma. The adenoma was smaller than the carcinomas, had no necrotic areas, was not invasive, and showed more evidence toward squamous and sebaceous differentiation (Fig. 33). The duct papilloma consisted of a large cystic space filled with cell debris and keratin and rimmed with projections of squamous epithelium with little evidence of sebaceous differentiation.

Preputial Gland Carcinomas

The third tumor type observed in the first 1,3-butadiene study at low incidences, but considered rare in mice and possibly related to treatment, was the preputial gland carcinoma (*7,9*). Preputial gland carcinomas were seen in three mice exposed to 625 ppm and two mice exposed to 1250 ppm. While no preputial gland carcinomas were observed prior to 65 weeks in the second study, at least three have been diagnosed after 65 weeks in each 625 ppm dose group exposed for 13 or 26 weeks. Grossly, they were described as masses ranging from 2 mm to 3.5 cm in diameter, pale or green, and firm or friable.

Histologically, the preputial gland carcinomas were tumors forming nests of epithelial cells at the periphery of a necrotic core. Occasionally the cells were large eosinophilic epithelial cells that were well differentiated toward squamous cells with keratin pearls or toward sebaceouslike cells. Seemingly more frequent were carcinomas with more anaplastic and pleomorphic basophilic epithelial cells. The nuclei tended to be smudged, and mitotic figures were common. The tumor cells aggressively invaded surrounding tissue and blood vessels forming nests that were separate from the main tumor mass (Fig. 34). Pulmonary metastasis was observed. Preputial gland adenomas were diagnosed in 2 of 2343 control male mice in a National Toxicology Program Data Base, while no carcinomas were observed in that same group (*9*).

Conclusion

Comparison of the results of 1,3-butadiene exposure of rodents to vinyl chloride is interesting. Vinyl chloride induced Zymbal gland tumors in rats (*22*). Zymbal gland tumors were associated with 1,3-butadiene exposure in rats and mice (*6–8*). Neuroblastomas were diagnosed in rats exposed to vinyl chloride (*22*), and neuroblastomas have been observed in mice exposed to 1,3-butadiene (*7,8*). Vinyl chloride exposure in mice caused an increased incidence of lung tumors and mammary adenocarcinomas with squamous metaplasia (*22*). 1,3-Butadiene exposure in mice was also associated with increased incidences of lung tumors and malignant mammary tumors, some of which had squamous differentiation. 1,3-Butadiene was also associated with increased incidences of mammary tumors in rats (*6*). Vinyl

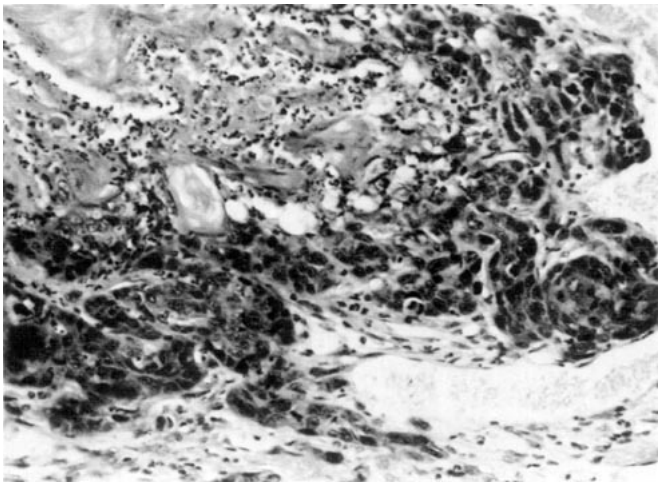

FIGURE 34. Preputial gland carcinoma that is highly anaplastic and invading a blood vessel. Original magnification, ×50.

chloride caused angiosarcomas in the liver and vascular tumors of other sites in rats and mice. One of the tumors was a fibroangioma of the heart (*22*). 1,3-Butadiene caused hemangiosarcomas in mice that were thought to be primary in the heart and metastatic to the liver.

The tumor processes discussed in this paper were those found to have statistically increased incidences in the first 1,3-butadiene study and those rare tumors possibly related to exposure but occurring at incidences below statistically significant levels. While not statistically significant, the rare tumor types may well be biologically significant.

Preliminary results from the second 1,3-butadiene study have demonstrated tumors similar, if not identical, to those observed in the first 1,3-butadiene study and present at lower exposure concentrations. 1,3-Butadiene induced a robust response of a large number of tumor types with a variety of morphologic patterns that were extremely complex in morphology and behavior.

REFERENCES

1. Kirk-Othmer Encyclopedia of Chemical Technology, Vol. 4, 3rd ed. John Wiley and Sons, New York, 1979, pp. 313–337.
2. de Meester, C., Mercier, M. and Poncelet, F. Mutagenic activity of butadiene, hexachlorobutadiene and isoprene. In: Industrial and Environmental Xenobiotics (I. Gut, M. Cikrt, and G. L. Plaa, Eds.), Springer-Verlag, New York, 1981, pp. 195–203.
3. Irons, R. D., Smith, C. N., Stillman, W. S., Shah, R. S., Steinhagen, W. H., and Leiderman, L. J. Macrocytic-megaloblastic anemia in male B6C3F$_1$ mice following chronic exposure to 1,3-butadiene. Toxicol. Appl. Pharmacol. 83: 95–100 (1986).
4. Tice, R. R., Boucher, R. Luke, C. A. and Shelby, M. D. Comparative cytogenetic analysis of bone marrow damage induced in male B6C3F$_1$ mice by multiple exposures to gaseous 1,3-butadiene. Environ. Mutagen. 9: 235–250 (1987).
5. Irons, R. D., Oshimura, M., and Barrett, J. C. Chromosome aberrations in mouse bone marrow cells following *in vivo* exposure to 1,3-butadiene. Carcinogenesis 8: 1711–1714 (1987).
6. Owen, P. E., Glaister, J. R., Gaunt, I. F. and Pullinger, D. H. Inhalation toxicity studies with 1,3-butadiene two year toxicity/carcinogenicity study in rats. Am. Ind. Hyg. Assoc. J. 48(5): 407–413 (1987).
7. NTP. Toxicology and Carcinogenesis Studies of 1,3-Butadiene in B6C3F$_1$ Mice. Technical Report No. 288. National Toxicology Program, Research Triangle Park, NC, 1984.
8. Huff, J. E., Melnick, R. L., Solleveld, H. A., Haseman, J. K., Powers, M., and Miller, R. A. Multiple organ carcinogenicity of 1,3-butadiene in B6C3F$_1$ mice after 60 weeks of inhalation exposure. Science 227: 548–549 (1985).
9. Haseman, J. K., Huff, J., and Boorman, G. A. Use of historical control data in carcinogenicity studies in rodents. Toxicol. Pathol. 12: 126 (1984).
10. Ward, J. M., Goodman, D. G., Squire, R. A., Chu, K. C., and Linhart, M. S. Neoplastic and non-neoplastic lesions in aging (C57BL/6NX C3H/HeN)F1 (B6C3F$_1$) mice. J. Natl. Cancer Inst. 63: 849–854 (1979).
11. Frith, C. H., and Wiley, L. D. Morphologic classification and correlation of incidence of hyperplastic and neoplastic hematopoietic lesions in mice with age. J. Gerontol. (36) 5: 534–545 (1981).
12. Irons, R. D., Stillman, W. S., Shah, R. S., and Morris, M. S. Phenotypic characterizations of 1,3-butadiene (BD)-induced thymic lymphoma in male B6C3F$_1$ mice. Toxicologist 6: 21 (1986).
13. Irons, R. D., Cathro, H. P., Stillman, W. S., Steinhagen, W. H., and Shah, R. S. Susceptibility to 1,3-butadiene-induced leukemogenesis correlates with endogenous ectropic retroviral background in the mouse. Toxicologist 8: 7 (1988).
14. Hoch-Ligeti, C., and Stewart, H. L. Cardiac tumors of mice. J. Natl. Cancer Inst. 72: 1449–1456 (1984).
15. Solleveld, H. A., Miller, R. A., Banas, D. A., and Boorman, G. A. Primary cardiac hemangiosarcomas induced by 1,3-butadiene in B6C3F$_1$ hybrid mice. Toxicol. Pathol. 16: 46–52 (1988).
16. Stewart, H. L., Dunn, T. B., Snell, K. C., and Deringer, M. K. Tumours of the respiratory tract. In: Pathology of Tumours in Laboratory Animals, Volume II—Tumours of the Mouse (V. S. Turusov, Ed.), IARC Scientific Publications, No. 23, International Agency for Research on Cancer, Lyon, France, 1979, pp. 251–288.
17. Kauffman, S. L., Alexander, L., and Sass, L. Histologic and ultrastructural features of the Clara cell adenoma of the mouse lung. Lab. Invest. 40: 708–716 (1979).
18. Squartini, F. Tumours of the mammary gland. In: Pathology of Tumours in Laboratory Animals, Volume II—Tumours of the Mouse (V. S. Turusov, Ed.), IARC Scientific Publications, No. 23, International Agency for Research on Cancer, Lyon, France, 1979, pp. 43–90.
19. Squire, R. A., Goodman, D. G., Valerio, M. G., Fredrickson, T., Strandberg, J. D., Levitt, M. H., Lingeman, C. H., Harshbarger, J. C., and Dowe, C. J. Tumors. In: Pathology of Domestic Animals, Vol. II (K. Benirschke, F. M. Garner, and T. C. Jones, Eds.), Springer-Verlag, New York, 1978, pp. 1052–1283.
20. Alison, R. H., and Morgan, K. T. Ovarian neoplasms in F344 rats and B6C3F$_1$ mice. Environ. Health Perspect. 73: 91–106 (1987).
21. Frith, C. H., and Ward, J. M. A morphologic classification of proliferative and neoplastic hepatic lesions in mice. J. Environ. Pathol. Toxicol. 3: 329–351 (1980).
22. Maltoni, C., and Lefemini, G. Carcinogenicity bioassay of vinyl chloride: current results. Ann. N.Y. Acad. Sci. 246: 195–219 (1975).